

# Mass bias evolution in tSZ cluster cosmology

Laura Salvati<sup>1\*</sup>, Marian Douspis<sup>1</sup>, Anna Ritz<sup>2</sup>, Nabila Aghanim<sup>1</sup>, and Arif Babul<sup>3</sup>

<sup>1</sup> Institut d'Astrophysique Spatiale, CNRS (UMR 8617) Université Paris-Sud, Bâtiment 121, Orsay, France

<sup>2</sup> Université Paris-Sud, Orsay, France

<sup>3</sup> Department of Physics and Astronomy, University of Victoria, Victoria, BC V8P 1A1, Canada

\*e-mail: [laura.salvati@ias.u-psud.fr](mailto:laura.salvati@ias.u-psud.fr)

## ABSTRACT

Galaxy clusters observed through the thermal Sunyaev-Zeldovich (tSZ) effect are a recent cosmological probe. The precision on the cosmological constraints is mainly affected by the current knowledge of clusters physics, that enters the analysis through the scaling relations. We study one of the most important sources of systematic uncertainties, the mass bias ( $1 - b$ ). We analyse the effects of a mass-redshift dependence, adopting a power-law parametrisation. We apply this parametrisation to the combination of tSZ number counts and power spectrum, finding a hint for redshift dependence that leads to an increasing value of the mass bias for higher redshift. We test the robustness of our results for different weak lensing calibrations and a discrete redshift dependence. We find our results to be dependent on the clusters sample that we are considering, in particular obtaining an inverse (decreasing) redshift dependence when neglecting  $z < 0.2$  clusters. We analyse the effects of this parametrisation on the combination of cosmic microwave background (CMB) primary anisotropies and tSZ galaxy clusters. We find a preferred constant value of mass bias,  $(1 - b) = 0.62 \pm 0.05$ , that is too low with respect to weak lensing and numerical simulations estimations. Therefore we conclude that this mass-redshift parametrisation does not help in solving the remaining discrepancy between CMB and tSZ clusters observations.

## 1. Introduction

Galaxy clusters are able to track the recent evolution of the large scale structure, describing the matter density field. Therefore, they represent an important cosmological probe.

In the last decades different observations of cluster samples in X-rays (Böhringer et al. 2017; Pacaud et al. 2018), optical (Rykoff et al. 2016) and millimetre wavelengths (Planck Collaboration 2014, 2016b; de Haan et al. 2016; Bocquet et al. 2018) have substantially improved the constraints on cosmological parameters obtained from this probe.

In this paper we consider galaxy clusters observed through the thermal Sunyaev-Zeldovich (tSZ hereafter) effect (Sunyaev & Zeldovich 1970). Latest cosmological analysis of tSZ galaxy clusters (Planck Collaboration 2014, 2016a,b; de Haan et al. 2016) have shown that the precision on the cosmological parameters is affected by systematic uncertainties, mainly related to cluster physics and theoretical assumptions, see e.g. discussion in McCarthy et al. 2003b,a; Poole et al. 2007; Hoekstra et al. 2012; Mahdavi et al. 2013; Ruan et al. 2013. In particular, we introduce uncertainties related to the calibration of the scaling relations between the survey observables and the real mass of the cluster, needed to extract cosmological information. A key element of these scaling relations is the mass bias. It arises from the assumption of hydrostatic equilibrium when estimating the cluster mass and it is therefore defined as the relation between the estimated and the real mass of the cluster. In practice, constraints on this parameter can be affected by all the unknowns related to the physics of the clusters. In order to quantify this bias, we use Weak Lensing (WL hereafter) mass reconstructions, which are supposed to provide an unbiased estimate of the true mass of the clus-

ter, see e.g. discussion in Mahdavi et al. 2008; Zhang et al. 2010; Mahdavi et al. 2013; Hoekstra et al. 2015; Smith et al. 2016.

In a previous paper (Salvati et al. 2018) we have shown that the well known discrepancy on cosmological parameters, in particular on  $\sigma_8$ , obtained from Cosmic Microwave Background radiation (CMB hereafter) primary anisotropies and tSZ observations (Planck Collaboration 2014, 2016a,b) is substantially reduced, thanks to the lower value of the optical depth provided by Planck Collaboration (2016d). This result has been confirmed also in the latest Planck release (Planck Collaboration 2018b). Nevertheless, we have shown that a tension is still present on the value of the mass bias, comparing estimation from tSZ probes alone and adding also CMB data. This remaining discrepancy can be related to the fact that we are assuming a constant value for the mass bias in the entire mass and redshift range of the cluster sample. Indeed, in Smith et al. (2016), the authors show that the mass calibration changes when considering clusters samples in different redshift ranges.

In this paper we analyse a possible variation for the mass bias, through an explicit mass-redshift parametrisation. We investigate the effects of this parametrisation on the CMB-tSZ mass bias discrepancy. In order to further explain our results and their impact on tSZ cosmological constraints, we analyse the effects of a redshift binned mass bias and different sample selections, in redshift and in signal-to-noise. We use measurements from the Planck satellite for the galaxy clusters number counts (Planck Collaboration 2016b), in combination with angular power spectrum of warm-hot gas, from Planck (Planck Collaboration 2016a) and the South Pole Telescope (SPT, George et al. 2015), starting from the analysis done in Salvati et al. (2018).

The paper is organised as follows: in section 2 we describe the approach we use in the analysis, presenting our results in sections 3 and 4. We discuss the results and derive our final conclusions in sections 5 and 6.

## 2. Method

In this analysis, we study the dependence of the mass bias with respect to mass and redshift, exploiting the combination of galaxy clusters number counts and power spectrum, following the approach described in Salvati et al. (2018).

We make use of the cluster sample provided by Planck Collaboration (2016c) (PSZ2 cosmo sample hereafter), consisting of 439 clusters obtained from the 65% cleanest part of the sky, in redshift range  $z = [0, 1]$  and above the signal-to-noise threshold of 6. Following the analysis done in Planck Collaboration (2016b), we sample on both redshift and signal-to-noise. We also use the Planck estimation of tSZ power spectrum Planck Collaboration (2016a), integrating in the redshift range  $z = [0, 3]$  and in the mass range  $M_{500} = [10^{13} h^{-1} M_{\odot}, 5 \cdot 10^{15} h^{-1} M_{\odot}]$ . We combine it with the estimation from SPT at  $\ell = 3000$  George et al. (2015).

We consider a parametric representation of the mass bias, such that the total varying mass bias can be defined as

$$(1-b)_{\text{var}} = (1-b) \cdot \left(\frac{M}{M_*}\right)^{\alpha_b} \cdot \left(\frac{1+z}{1+z_*}\right)^{\beta_b}, \quad (1)$$

where  $(1-b)$  is an amplitude,  $M_* = 6 \cdot 10^{14} M_{\odot}$  to be consistent with the pivot mass of the scaling relations (see Eqs. (7) and (8) in Planck Collaboration 2016b) and  $z_* = 0.22$  is the median value of the clusters catalogue that we are considering. Following the analysis in Salvati et al. (2018), we apply a WL prior from the Canadian Cluster Comparison Project (CCCP, Hoekstra et al. 2015) on the total quantity  $(1-b)_{\text{var}}$  evaluated at the mean mass and redshift for the sample considered in the CCCP analysis.

For CMB data, we exploit the new results from the Planck collaboration (Planck Collaboration 2018a,b). The new Planck likelihood is not public yet. In order to reproduce the constraints on the cosmological parameters  $\Omega_m$  (matter density) and  $\sigma_8$  (normalization of the matter power spectrum), we mimic the Planck 2018 likelihood assuming a Gaussian prior on the optical depth,  $\tau = 0.054 \pm 0.007$  (Planck Collaboration 2018b). We check that the 68% confidence level (c.l. from now on) constraints that we obtain for  $\Omega_m$  and  $\sigma_8$  are in agreement with the ones reported in Planck Collaboration (2018b).

When not considering CMB data, we add to tSZ data also results from baryon acoustic oscillations (BAO) from Anderson et al. (2014), but for brevity in the text we refer to this dataset combination simply as "tSZ data". In the entire analysis we make use of mass function from Tinker et al. (2008).

Results discussed in the next section are obtained using Monte Carlo Markov Chains (MCMC). We sample at the same time on cosmological and mass bias parameters, together with the other scaling relation parameters. We use the November 2016 version of the publicly available package cosmomc Lewis & Bridle (2002). All the details on how the likelihoods for tSZ number counts and power spectrum are combined are discussed in Salvati et al. (2018).

In order to check the consistency of our results, we perform several tests. We analyse the effect of a second significantly different WL calibration, from the Weighting the Giants project (WtG, von der Linden et al. 2014), applying the prior on the total  $(1-b)_{\text{var}}$  quantity evaluated at the mean mass and redshift for the WtG catalogue. We then consider a discrete redshift dependence for the mass bias, dividing the entire redshift range of the PSZ2 cosmo sample in different bins, with different mass bias values. We check how the results change for different redshift and signal-to-noise cuts in the cluster catalogue.

## 3. Results

We report the results obtained for the mass-redshift parametrisation of the mass bias. We analyse only the  $\Lambda$ CDM scenario of cosmology. Regarding the cosmological parameters, we focus on the total matter density  $\Omega_m$  and the normalization of the matter power spectrum, described through  $\sigma_8$ .

We compare the "standard" scenario (i.e. mass bias constant in the entire mass and redshift range  $(1-b)_{\text{var}} = (1-b)$ , labelled as "+(1-b)" only) with the one adding the mass and redshift dependencies, quantified by the  $\alpha_b$  and  $\beta_b$  parameters. In this second case, we consider both the case where the amplitude in Eq. (1) is varying or fixed to the value found in the "standard" scenario for the tSZ data combination, i.e.  $(1-b) = 0.75$ .

### 3.1. tSZ power spectrum and number counts

We start discussing the  $C_{\ell}^{\text{tSZ}} + \text{NC}^{\text{tSZ}} + \text{BAO}$  data combination. The two-dimensional probability distributions in the  $(\Omega_m, \sigma_8)$  parameter plane are shown in Fig. 1 for the standard scenario ("+(1-b)", red contours), allowing for the mass and redshift variation (" $+\alpha_b + \beta_b$ ", green filled contours) and for the complete parameters combination ("+(1-b) +  $\alpha_b + \beta_b$ ", blue filled contours). The 68% c.l. constraints are reported in Tab. 1 for all the parameters combinations.

Allowing for  $\alpha_b$  and  $\beta_b$  to vary enlarges the constraints towards higher values of  $\Omega_m$ . This is mainly due to the degeneracy between the matter density and the redshift dependence, as shown in Fig. 2. Indeed, we find a hint for redshift dependence, having  $\beta_b$  consistent with 0 only within  $2\sigma$  and pointing towards values of the total  $(1-b)_{\text{var}}$  quantity increasing with redshift. The one-dimensional probability distributions for  $\beta_b$  are shown in Fig. 3 for the different dataset combinations. Regarding the  $\alpha_b$  parameter, we are not able to find an explicit mass dependence, since we always obtain  $\alpha_b$  consistent with 0 within  $1\sigma$ . This can be due also to the strong degeneracy that we find between the amplitude  $(1-b)$  and  $\alpha_b$ , as it can be seen in the scatter plot in Fig. 4, left panel.

We evaluate the total  $(1-b)_{\text{var}}$  quantity and report it in Fig. 5 (green and blue curves), where the shaded areas represent the estimated  $1\sigma$  error. In order to stress the effect of the mass and redshift variation, we show the trend for  $(1-b)_{\text{var}}$  at fixed values of redshift and mass respectively, considering in each case the lowest and highest values in the cluster catalogue range. From these results it is easy to see the combined effect of mass and redshift dependence on the evolution of the mass bias.

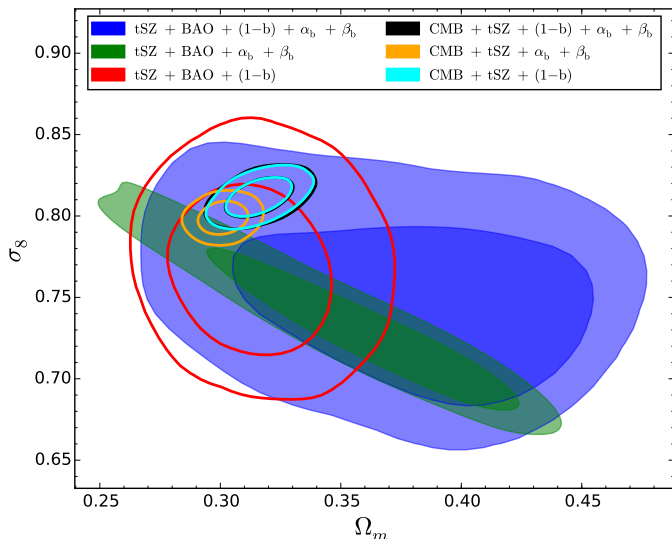


**Fig. 1.** Two-dimensional probability distribution for the parameters  $\Omega_m$  and  $\sigma_8$ , showing 68% and 95% c.l. We show the tSZ+BAO data, with  $tSZ = C_\ell^{tSZ} + NC^{tSZ}$ ; varying only the amplitude in Eq. (1) (red contours), adding the mass and redshift dependence (blue filled contours) and fixing the amplitude (green filled contours). We show the same combinations adding CMB data (cyan, black and orange contours).

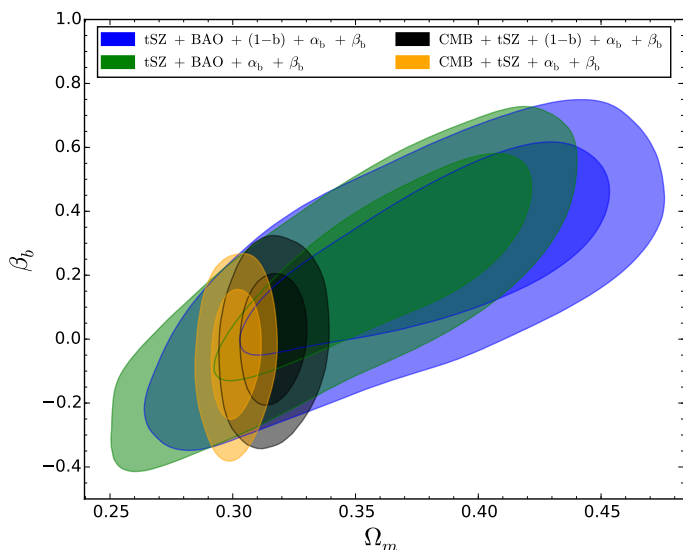


**Fig. 2.** Two-dimensional probability distributions for the parameters  $\Omega_m$  and  $\beta_b$ , showing 68% and 95% c.l. We show tSZ+BAO results, with  $tSZ = C_\ell^{tSZ} + NC^{tSZ}$ , for the complete mass bias parameters combination (blue) and fixing the amplitude (green). We report the same combinations when adding also CMB data (black and orange respectively).

### 3.2. Comparison between CMB and tSZ data

We start comparing results on the  $(\Omega_m, \sigma_8)$  parameter plane for the "standard" scenario. [Planck Collaboration \(2018b\)](#) provides the following 68% c.l. constraints, from the baseline Planck TT,TE,EE+lowE+lensing:  $\Omega_m = 0.315 \pm 0.007$  and  $\sigma_8 = 0.811 \pm 0.006$ . Regarding the combination with tSZ data (considering number counts only in this case), they provide the value for the mass bias  $(1-b) = 0.62 \pm 0.03$ . Comparing these values with the ones reported here in

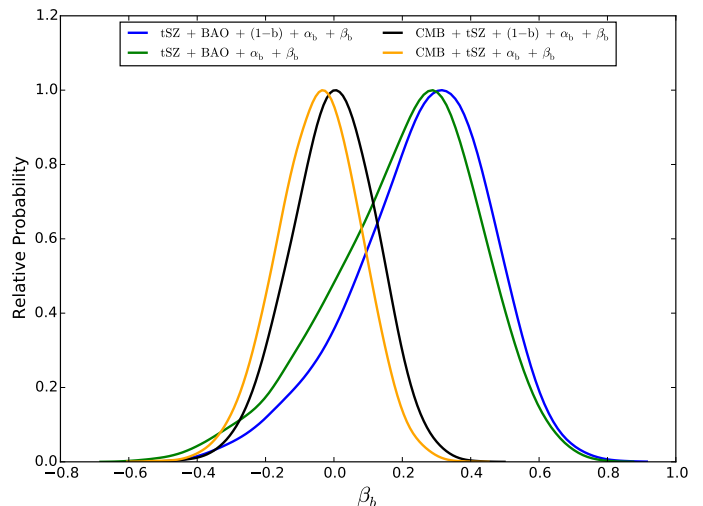


**Fig. 3.** One dimensional probability distributions for the  $\beta_b$  parameter. We show tSZ+BAO results, with  $tSZ = C_\ell^{tSZ} + NC^{tSZ}$ , for the complete mass bias parameters combination (blue) and fixing the amplitude (green). We report the same combinations when adding also CMB data (black and orange respectively).

Tab. 1 for the CMB +  $C_\ell^{tSZ} + NC^{tSZ} + (1-b)$  scenario, we find a complete agreement, showing the strongest constraining power of tSZ number counts with respect to the power spectrum.

Two dimensional probability distributions in the  $(\Omega_m, \sigma_8)$  parameter plane are shown in Fig. 1 for the standard scenario ("+(1-b)", cyan contours), opening for the mass and redshift variation ("+ $\alpha_b + \beta_b$ ", orange contours) and for the complete parameters combination ("+(1-b) +  $\alpha_b + \beta_b$ ", black contours). The 68% c.l. constraints are reported in Tab. 1.

We can now compare results for CMB +  $C_\ell^{tSZ} + NC^{tSZ} + (1-b)$  with those considering only tSZ data, i.e.  $C_\ell^{tSZ} + NC^{tSZ} + BAO + (1-b)$ . As it has been already discussed in [Salvati et al. \(2018\)](#) and in [Planck Collaboration \(2018b\)](#), the lower value of the optical depth  $\tau$  helps in reducing the discrepancy between tSZ and CMB data, at least on the  $\sigma_8$  parameter. Given the degeneracy between the  $\sigma_8$  parameter and the mass bias, the lower value of  $\tau$  helps also in partly reducing the discrepancy on this latter quantity. Nevertheless, current CMB+tSZ data combination prefers a value of the mass bias,  $(1-b) = 0.62 \pm 0.04$ , that is still only marginally consistent with current simulations and WL calibrations, see e.g. the collection of results reported in [Salvati et al. \(2018, Fig. 10\)](#).

We therefore analyse if the mass-redshift parametrisation proposed in Eq. 1 can allow for a convergence of CMB and tSZ results towards higher values of the mass bias. The results from CMB +  $C_\ell^{tSZ} + NC^{tSZ}$  data combination confirm the strongest constraining power of CMB data. Indeed, for the complete case with varying  $(1-b) + \alpha_b + \beta_b$ , results are completely in agreement with the standard scenario when only  $(1-b)$  is varying, with  $\alpha_b$  and  $\beta_b$  being consistent with 0. Fixing the amplitude to  $(1-b) = 0.75$  does not provide a good fit to data. Indeed we find a worst  $\chi^2$  ( $\chi^2_{\alpha+\beta} = 2919$ ) with respect to the other parameters combinations ( $\chi^2_{(1-b)} = \chi^2_{(1-b)+\alpha+\beta} = 2912$ )

In Fig. 4, right panel, we report the two dimensional probability distribution for  $(\alpha_b, \beta_b)$  at different values of the amplitude  $(1 - b)$ . We find a mild correlation between  $\alpha_b$  and  $\beta_b$ . Furthermore, we see that we are never able to reach values  $(1 - b) \sim 0.8$ , for any combination of  $(\alpha_b, \beta_b)$ .

We conclude comparing the results for the total  $(1 - b)_{\text{var}}$  quantity, for the complete  $(1 - b) + \alpha_b + \beta_b$  scenario. In Fig. 5 we show also the results for the CMB+tSZ data combination (red and magenta lines and shaded areas). From these results we can see that adding CMB data keeps the value of  $(1 - b)_{\text{var}}$  almost constant in mass and redshift, while results for tSZ data show a variation. It is furthermore clear that the adopted mass-redshift parametrisation does not help in solving the remaining tension on the mass bias between CMB and tSZ data.

## 4. Robustness tests

In order to further understand our results, in particular the hint for redshift dependence leading to an increasing value of  $(1 - b)_{\text{var}}$  for higher redshift for tSZ data, we perform several analyses. The aim is to understand if the obtained constraints may depend on the choice of the WL calibration, the mass-redshift dependence description or the sample selection.

Before showing these results, we analyse the effect of the tSZ power spectrum. Indeed, the wider redshift range covered by tSZ power spectrum measurements ( $z = [0, 3]$ ) could be the cause for the increasing trend of  $(1 - b)_{\text{var}}$  with redshift. We compare the results for the complete  $C_\ell^{\text{tSZ}} + \text{NC}^{\text{tSZ}} + \text{BAO}$  combination with the ones obtained from  $\text{NC}^{\text{tSZ}} + \text{BAO}$ , the latter being reported in Tab. 2, upper panel. We find a complete agreement for the two datasets combinations, in particular for the constraints on  $\beta_b$ . Therefore we confirm that, also in the " $(1 - b) + \alpha_b + \beta_b$ " scenario, tSZ power spectrum provides a lower constraining power with respect to number counts, as it is already shown for the "standard" scenario in Salvati et al. (2018).

Hence, for all the following tests we decide to focus only the  $\text{NC}^{\text{tSZ}} + \text{BAO}$  combination.

### 4.1. Effect of WL priors

We compare results for two significantly different WL calibrations. In particular, we compare the baseline analysis, adopting the CCCP calibration, with results obtained using WtG prior. We choose WtG as a comparison check, since they provide a lower value for the mass bias,  $(1 - b)_{\text{WtG}} = 0.688 \pm 0.072$ , more in agreement with the expected value from the  $\text{CMB} + C_\ell^{\text{tSZ}} + \text{NC}^{\text{tSZ}}$  combination. The constraints are reported in Tab. 2, upper panel, and we show the results for the  $(\Omega_m, \sigma_8)$  parameter plane in Fig. 6. As a reference, we report also results for the "standard" case, when the mass-redshift dependence is not allowed. We can clearly see the effect of the different WL calibrations, with results from WtG slightly pointing towards higher values of  $\sigma_8$  and providing a thinner two-dimensional distribution, due to the smaller error bars on the  $(1 - b)_{\text{WtG}}$ . Nevertheless, we find a general agreement between the two calibrations, for both scenarios  $\text{NC}^{\text{tSZ}} + \text{BAO} + (1 - b)$  and  $\text{NC}^{\text{tSZ}} + \text{BAO} + (1 - b) + \alpha_b + \beta_b$ . In particular,

we find the same hint for redshift dependence, having  $\beta_b = 0.24_{-0.18}^{+0.24}$  for CCCP and  $\beta_b = 0.27_{-0.16}^{+0.22}$  for WtG. We conclude therefore that the our results on the redshift dependence are independent of the choice of the WL calibration.

### 4.2. Binning in redshift

We now analyse results from the discrete redshift dependence for the mass bias, dividing the redshift range,  $z = [0, 1]$ , in three bins. Also in this case, we compare the effect of CCCP and WtG calibrations, considering the  $\text{NC}^{\text{tSZ}} + \text{BAO}$  combination. For this analysis, in each redshift bin, we do not re-evaluate the WtG and CCCP cluster masses, but we find the value of  $(1 - b)$  that allows for consistency between WL and tSZ results. We choose the binning considering the redshift distributions of the two CCCP and WtG subsamples, such that, for each calibration, the majority of the clusters is included in the second bin, that also encompasses the median redshift of the sample. We then mimic the two calibrations by adding a gaussian prior on the mass bias parameter in the second redshift bin. The number of clusters in the chosen redshift bins for each calibration are reported in Tab. 3, with the relative prior for the mass bias. Results are reported in Tab. 2, lower panel. As expected, results obtained with the WtG calibration slightly point towards higher values of  $\sigma_8$ , as shown in Fig. 7. Nevertheless, we find a general agreement between the two calibrations.

We compare this redshift binning analysis with the mass-redshift parametrisation, focusing on results obtained with the CCCP calibration. In Fig. 8 we show the two dimensional probability distributions in the  $(\Omega_m, \sigma_8)$  plane for the two cases. We find that also the redshift binning analysis provide constraints for  $\Omega_m$  shifted towards higher values. We now focus on the constraints for the mass bias parameters in each redshift bin. The one-dimensional probability distributions are shown in Fig. 9. We find a mild confirmation for the increasing value of the mass bias for higher redshift. Indeed, results for the second and third bin point toward higher values, showing only a marginal consistency, within  $2\sigma$ , with the first bin.

### 4.3. Selection effects

We conclude this section by taking into account possible catalogue selection effects. In particular, we consider different subsamples of the entire PSZ2 cosmo sample. As described in section 2, the latter is selected with a signal-to-noise threshold  $q_{\text{min}} = 6$  and counts 439 clusters. As a comparison, following the analysis in Planck Collaboration (2016b), we consider two other thresholds,  $q_{\text{min}} = 7$  and  $q_{\text{min}} = 8.5$ , which provide samples of 339 and 216 clusters respectively. We label these samples as "PSZ2 A" and "PSZ2 B". We consider also a different range in redshift, selecting only clusters with  $z \gtrsim 0.2$ . This cut provides a sample of 225 clusters, which we label "PSZ2 C". As a reference, the specifics of the different samples are reported in Tab. 4.

We compare results for CCCP and WtG calibrations on the  $\text{NC}^{\text{tSZ}} + \text{BAO} + (1 - b) + \alpha_b + \beta_b$  combination. The constraints are reported in Tab. 5, where for compari-

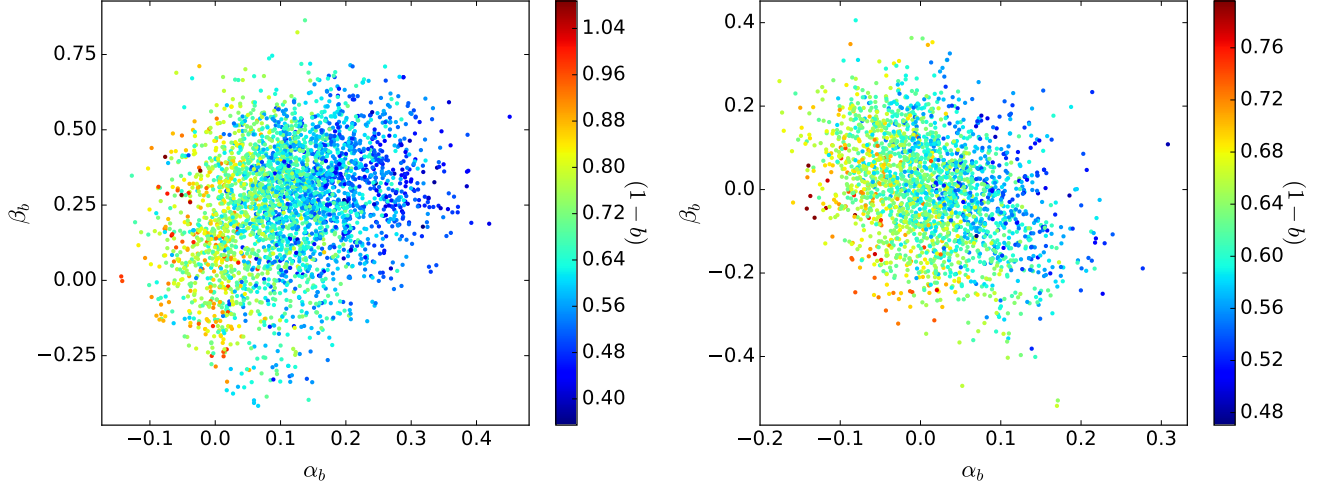


**Fig. 4.** Scatter plots for  $(\alpha_b, \beta_b)$  parameters at different values of the amplitude  $(1-b)$ . We show results for  $C_\ell^{\text{tSZ}} + \text{NC}^{\text{tSZ}} + \text{BAO} + (1-b) + \alpha_b + \beta_b$  (left panel) and  $\text{CMB} + C_\ell^{\text{tSZ}} + \text{NC}^{\text{tSZ}} + (1-b) + \alpha_b + \beta_b$  (right panel).

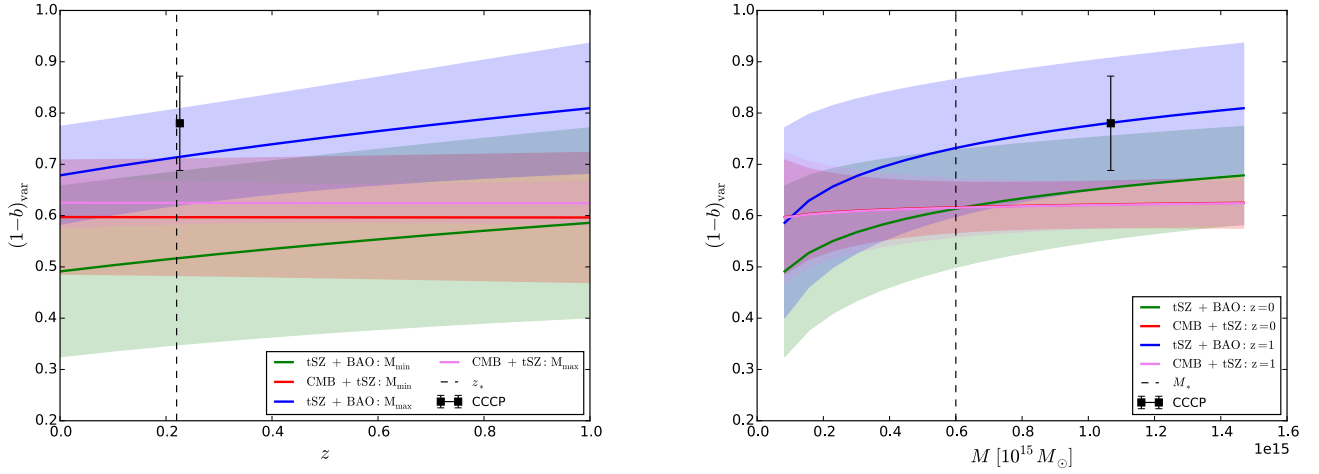


**Fig. 5.** Redshift (left panel) and mass (right panel) variation of  $(1-b)_{\text{var}}$  at fixed values of mass and redshift respectively. We show results for the combinations  $C_\ell^{\text{tSZ}} + \text{NC}^{\text{tSZ}} + \text{BAO} + (1-b) + \alpha_b + \beta_b$  (labelled as "tSZ + BAO") and  $\text{CMB} + C_\ell^{\text{tSZ}} + \text{NC}^{\text{tSZ}} + (1-b) + \alpha_b + \beta_b$  (labelled as "CMB + tSZ").

Datasets	$\Omega_m$	$\sigma_8$	$(1-b)$	$\alpha_b$	$\beta_b$
$C_\ell^{\text{tSZ}} + \text{NC}^{\text{tSZ}} + \text{BAO} + (1-b)$	$0.315^{+0.020}_{-0.024}$	$0.769^{+0.029}_{-0.036}$	$0.748 \pm 0.094$	0	0
$C_\ell^{\text{tSZ}} + \text{NC}^{\text{tSZ}} + \text{BAO} + (1-b) + \alpha_b + \beta_b$	$0.381^{+0.060}_{-0.033}$	$0.749^{+0.030}_{-0.039}$	$0.65^{+0.10}_{-0.13}$	$0.11^{+0.08}_{-0.10}$	$0.25^{+0.23}_{-0.16}$
$C_\ell^{\text{tSZ}} + \text{NC}^{\text{tSZ}} + \text{BAO} + \alpha_b + \beta_b$	$0.356^{+0.053}_{-0.030}$	$0.732^{+0.021}_{-0.040}$	0.75	$0.052 \pm 0.058$	$0.21^{+0.25}_{-0.17}$
$\text{CMB} + C_\ell^{\text{tSZ}} + \text{NC}^{\text{tSZ}} + (1-b)$	$0.316 \pm 0.009$	$0.812 \pm 0.007$	$0.623^{+0.033}_{-0.039}$	0	0
$\text{CMB} + C_\ell^{\text{tSZ}} + \text{NC}^{\text{tSZ}} + (1-b) + \alpha_b + \beta_b$	$0.316 \pm 0.009$	$0.812 \pm 0.007$	$0.616 \pm 0.046$	$0.016^{+0.067}_{-0.078}$	$0^{+0.14}_{-0.12}$
$\text{CMB} + C_\ell^{\text{tSZ}} + \text{NC}^{\text{tSZ}} + \alpha_b + \beta_b$	$0.301 \pm 0.006$	$0.799 \pm 0.006$	0.75	$-0.069^{+0.053}_{-0.060}$	$-0.04 \pm 0.12$

**Table 1.** 68% c.l. constraints for cosmological and mass bias parameters, for the different dataset combinations.

Datasets	$\Omega_m$	$\sigma_8$	$(1-b)$	$\alpha_b$	$\beta_b$
CCCP: NC <sup>tSZ</sup> + BAO + $(1-b)$	$0.314 \pm 0.023$	$0.769^{+0.028}_{-0.034}$	$0.751 \pm 0.093$	0	0
CCCP: NC <sup>tSZ</sup> + BAO + $(1-b) + \alpha_b + \beta_b$	$0.374^{+0.065}_{-0.035}$	$0.752^{+0.033}_{-0.040}$	$0.66^{+0.10}_{-0.14}$	$0.10 \pm 0.10$	$0.24^{+0.24}_{-0.18}$
WtG: NC <sup>tSZ</sup> + BAO + $(1-b)$	$0.315 \pm 0.022$	$0.780^{+0.022}_{-0.025}$	$0.714 \pm 0.056$	0	0
WtG: NC <sup>tSZ</sup> + BAO + $(1-b) + \alpha_b + \beta_b$	$0.389^{+0.051}_{-0.027}$	$0.754^{+0.024}_{-0.030}$	$0.611^{+0.074}_{-0.085}$	$0.131^{+0.079}_{-0.096}$	$0.27^{+0.22}_{-0.16}$
	$\Omega_m$	$\sigma_8$	$(1-b)_1$	$(1-b)_2$	$(1-b)_3$
CCCP: NC <sup>tSZ</sup> + BAO	$0.371^{+0.028}_{-0.034}$	$0.733^{+0.028}_{-0.037}$	$0.655 \pm 0.078$	$0.775 \pm 0.092$	$0.751 \pm 0.095$
WtG: NC <sup>tSZ</sup> + BAO	$0.376 \pm 0.036$	$0.759^{+0.031}_{-0.037}$	$0.585^{+0.068}_{-0.062}$	$0.692^{+0.070}_{-0.072}$	$0.670^{+0.075}_{-0.082}$

**Table 2.** 68% c.l. constraints for cosmological and mass bias parameters, for the different dataset combinations.

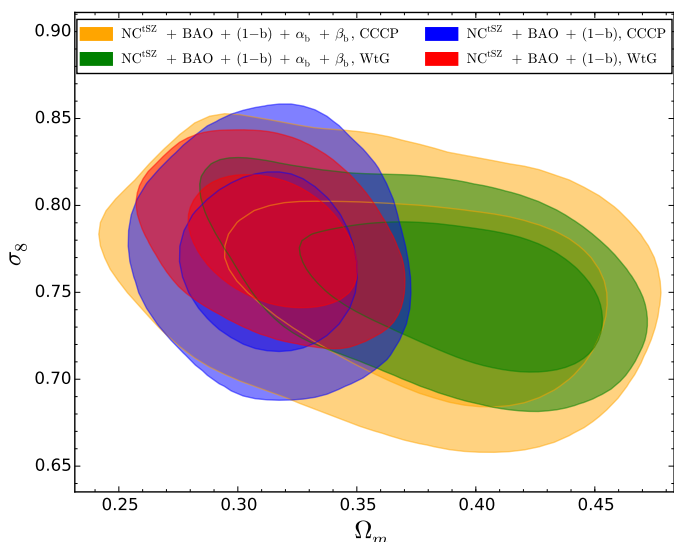


**Fig. 6.** Two-dimensional probability distribution for the parameters  $\Omega_m$  and  $\sigma_8$ , showing 68% and 95% c.l.. We compare results for the CCCP and WtG calibrations for the standard scenario when only  $(1-b)$  is varying (blue and red filled contours respectively) and for the " $(1-b) + \alpha_b + \beta_b$ " scenario (orange and green filled contours).

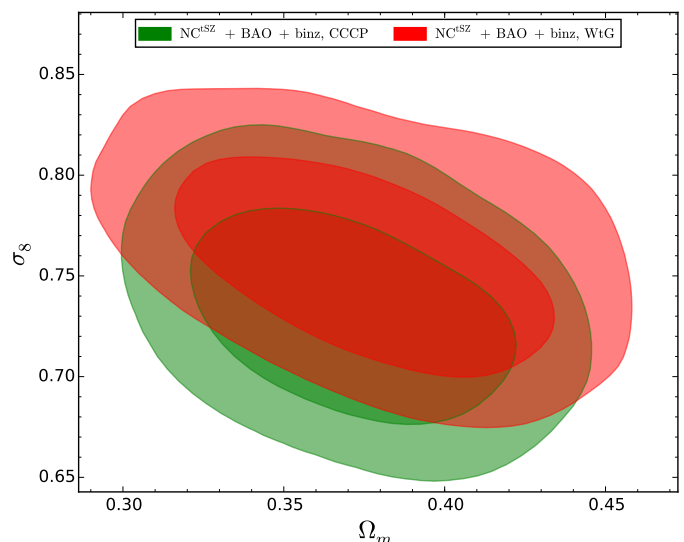


**Fig. 7.** Two-dimensional probability distributions for  $\Omega_m$  and  $\sigma_8$ , showing 68% and 95% c.l.. We compare results for NC<sup>tSZ</sup> + BAO for the redshift binning analysis considering CCCP (green) and WtG calibration (red).

	bin 1 [0, 0.2]	bin 2 [0.2, 0.5]	bin 3 [0.5, 1]	$(1-b)_2$
CCCP	6	11	1	$0.78 \pm 0.092$
WtG	3	21	1	$0.688 \pm 0.072$
PSZ2 cosmo sample	209	200	23	

**Table 3.** Number of galaxy clusters per redshift bin, for the different WL calibrations, compared with the Planck cosmological sample (Planck Collaboration 2016b).

son purposes we report again the constraints for the entire PSZ2 cosmo catalogue. For each sample we find a general agreement between the two WL calibrations. Therefore, we focus here only on results obtained adopting the CCCP calibration.

Focusing on the  $\alpha_b$  and  $\beta_b$  parameters, we see how results change considering the different samples. In particular, changing the signal-to-noise threshold shifts the  $\alpha_b$  parameter from being completely consistent with 0 ( $\alpha_b = 0.10 \pm 0.10$  at  $q_{\min} = 6$ ) to provide a strong hint for mass dependence ( $\alpha_b = 0.38^{+0.12}_{-0.03}$  at  $q_{\min} = 8.5$ ), pointing the  $(1-b)_{\text{var}}$  quantity to increase with mass. On the contrary, the  $\beta_b$  parameter is shifted towards lower values, in agreement with 0, from  $\beta_b = 0.24^{+0.24}_{-0.18}$  at  $q_{\min} = 6$  to  $\beta_b = -0.24^{+0.36}_{-0.38}$  at  $q_{\min} = 8.5$ .

When considering the different redshift ranges, on the one hand  $\alpha_b$  remains consistent with 0, with  $\alpha_b = 0.10 \pm 0.10$  for  $z$  in  $[0, 1]$  and  $\alpha_b = 0.04 \pm 0.10$  for  $z$  in  $[0.2, 1]$ . On the

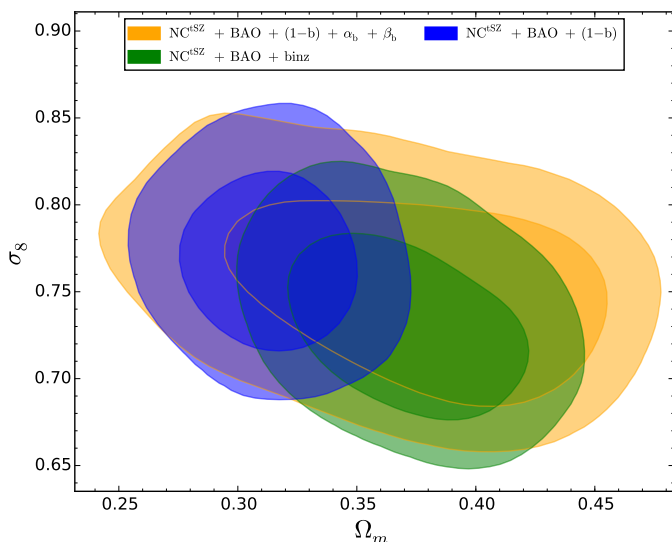


**Fig. 8.** Two-dimensional probability distributions for  $\Omega_m$  and  $\sigma_8$ . We show the comparison between the complete combination  $\text{NC}^{\text{tSZ}} + \text{BAO} + (1-b) + \alpha_b + \beta_b$  (orange) and results from the binning in redshift (green). As a reference, we show in blue the constraints for the "standard" case  $\text{NC}^{\text{tSZ}} + \text{BAO} + (1-b)$ . All results are obtained considering the CCCP calibration.

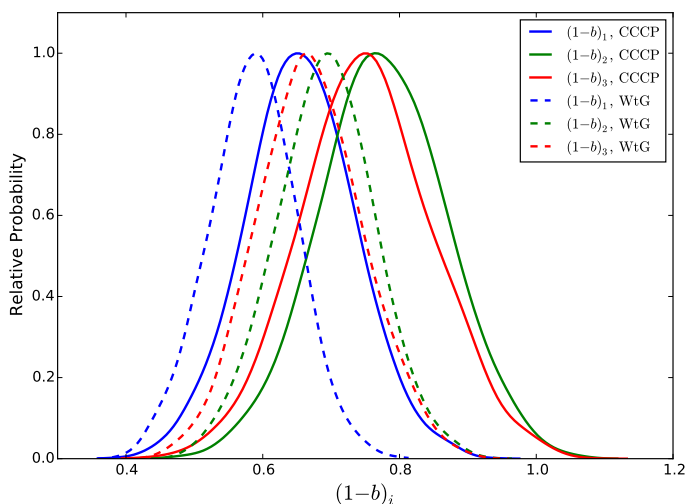


**Fig. 9.** One dimensional posterior distributions for the mass bias parameter in each redshift bin, for the  $\text{NC}^{\text{tSZ}} + \text{BAO}$  combination. We report results for CCCP (solid line) and WtG (dashed line) calibration.

other hand,  $\beta_b$  changes from  $\beta_b = 0.24^{+0.24}_{-0.18}$  for  $z$  in  $[0, 1]$  to  $\beta_b = -0.09^{+0.23}_{-0.17}$  for  $z$  in  $[0.2, 1]$ .

Focusing in particular on the redshift dependence, we show in Fig. 10 the  $(1-b)_{\text{var}}$  variation for the PSZ2 cosmo and PSZ2 C samples. We can clearly see that neglecting the low redshift clusters induces an opposite redshift dependence, leading to a decreasing trend of  $(1-b)_{\text{var}}$  for higher redshift.

We therefore conclude that constraints on the mass-redshift dependence for the mass bias are completely dependent on the sample that we are considering.

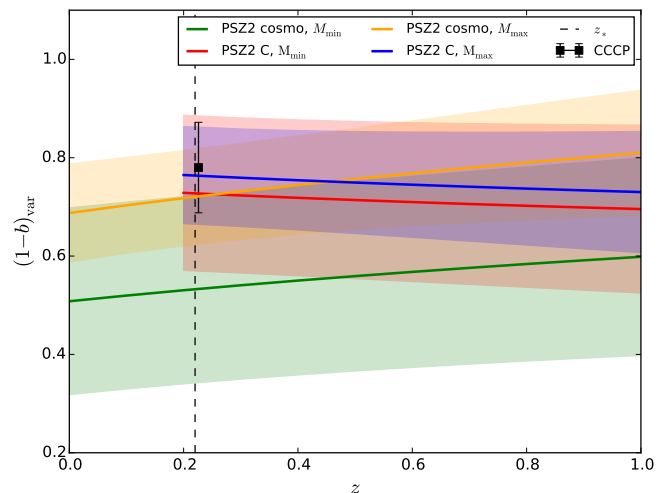


**Fig. 10.** Redshift variation of  $(1-b)_{\text{var}}$  at fixed values of mass. We compare results for the complete PSZ2 cosmo sample and the PSZ2 C sample, obtained selecting  $z \gtrsim 0.2$  clusters, in both cases adopting CCCP calibration.

Catalogue	$q_{\text{min}}$	$z$ range	n° of clusters
PSZ2 cosmo	6	$[0, 1]$	439
PSZ2 A	7	$[0, 1]$	339
PSZ2 B	8.5	$[0, 1]$	216
PSZ2 C	6	$[0.2, 1]$	225

**Table 4.** Characteristics of the different clusters samples.

## 5. Discussion

Calibration of the mass bias and its possible mass and redshift dependence have raised lot of interest in the community. Planck collaboration provided such a wide galaxy clusters catalogue that many authors have contributed with evaluations of clusters mass and with possible estimation of mass and redshift dependence for the mass bias, selecting different subsamples of the catalogue, see e.g. (von der Linden et al. 2014; Hoekstra et al. 2015; Okabe & Smith 2016; Sereno & Ettori 2015a; Smith et al. 2016; Penna-Lima et al. 2017; Sereno et al. 2017) and a collection of measurements in Salvati et al. (2018). Indeed, given how the discrepancy on cosmological parameters between tSZ probes and CMB data has been partially solved thanks to new measurements of the optical depth, the correct description of the mass bias remains one of the open issues when using galaxy clusters as a cosmological probe.

The mass bias is generally introduced to quantify any departures from the assumption of hydrostatic equilibrium when evaluating clusters masses with X-rays and tSZ observations. The uncertainties in the evaluation of the mass bias can be related to the description of cluster physics (e.g. baryonic effects, processes leading to non-thermal pressure contributions, magnetic field) or to experimental uncertainties in tSZ and X-rays measurements. Hydrodynamical simulations provide an alternative estimation of this quantity,

NC <sup>tSZ</sup> + BAO + (1 - b) + $\alpha_b$ + $\beta_b$	$\Omega_m$	$\sigma_8$	(1 - b)	$\alpha_b$	$\beta_b$
PSZ2 cosmo, CCCP	$0.374^{+0.065}_{-0.035}$	$0.752^{+0.033}_{-0.040}$	$0.66^{+0.10}_{-0.14}$	$0.10 \pm 0.10$	$0.24^{+0.24}_{-0.18}$
PSZ2 cosmo, WtG	$0.389^{+0.051}_{-0.027}$	$0.754^{+0.024}_{-0.030}$	$0.611^{+0.074}_{-0.085}$	$0.131^{+0.079}_{-0.096}$	$0.27^{+0.22}_{-0.16}$
PSZ2 A, CCCP	$0.380^{+0.062}_{-0.037}$	$0.772^{+0.031}_{-0.038}$	$0.51 \pm 0.10$	$0.29 \pm 0.11$	$0.01^{+0.31}_{-0.24}$
PSZ2 A, WtG	$0.380^{+0.048}_{-0.040}$	$0.768^{+0.024}_{-0.030}$	$0.510^{+0.059}_{-0.081}$	$0.29 \pm 0.10$	$0.02^{+0.29}_{-0.22}$
PSZ2 B, CCCP	$0.364^{+0.054}_{-0.040}$	$0.770^{+0.032}_{-0.039}$	$0.444^{+0.057}_{-0.084}$	$0.38^{+0.12}_{-0.03}$	$-0.22^{+0.39}_{-0.32}$
PSZ2 B, WtG	$0.357^{+0.057}_{-0.048}$	$0.764^{+0.027}_{-0.031}$	$0.470^{+0.049}_{-0.080}$	$0.37^{+0.13}_{-0.04}$	$-0.24^{+0.36}_{-0.38}$
PSZ2 C, CCCP	$0.378^{+0.048}_{-0.036}$	$0.740^{+0.034}_{-0.044}$	$0.74^{+0.12}_{-0.15}$	$0.04 \pm 0.10$	$-0.09^{+0.23}_{-0.17}$
PSZ2 C, WtG	$0.382^{+0.051}_{-0.036}$	$0.755^{+0.030}_{-0.033}$	$0.68 \pm 0.10$	$0.05^{+0.09}_{-0.11}$	$-0.11^{+0.24}_{-0.20}$

**Table 5.** 68% c.l. constraints for cosmological and mass bias parameters, for the different dataset combinations.

$(1 - b) \sim 0.8$ , with the main uncertainties being related to the identification and evaluation of the different processes leading to non-thermal pressure contributions, see e.g. [Biffi et al. \(2016\)](#) and a collection of references in [Planck Collaboration \(2014\)](#).

Given this complex scenario, we propose a simple and empirical mass and redshift parametrisation for the mass bias. In discussing the results, we focus both on the constraints on the mass bias itself and on the effects on the CMB-tSZ discrepancy. Since the strongest constraining power of CMB data does not allow to have any mass or redshift variation, for the first part of the discussion we focus only on results from tSZ data.

In previous sections we have shown on the one hand that, when considering the entire PSZ2 cosmo catalogue, we find a hint of redshift dependence, having the  $\beta_b$  parameter being consistent with 0 only within  $2\sigma$ . In particular, we find the total value of  $(1 - b)_{\text{var}}$  to be increasing with redshift. On the other hand, we are not able to explicitly constrain a mass dependence for the mass bias through the  $\alpha_b$  parameter, given the strong degeneracy in the  $(\alpha_b, (1 - b))$  plane.

In order to provide a more complete analysis, we compare results from two WL calibrations. We select the CCCP and WtG analysis, to highlight how lower and higher values of the mass bias affect the constraints on  $\Omega_m$  and especially  $\sigma_8$ . When comparing these results it is important to recover how the calibrations are estimated. For all the details, we refer to the single analysis ([Hoekstra et al. 2015](#); [von der Linden et al. 2014](#)). We only recall here that the different works consider diverse subsamples of the entire Planck cosmological catalogue, with different number of clusters, mass and redshift range and yet with some overlapping of objects between the different selections. Furthermore, the lensing mass extraction methodologies differ from one evaluation to the other. Nevertheless, the interesting result lies in the fact that, even considering different WL calibrations, we find the same increasing trend towards high redshift of  $(1 - b)_{\text{var}}$ .

This result is also confirmed when we divide the redshift range of the PSZ2 cosmo sample in three bins and evaluate

the mass bias in each bin. Indeed, we find the  $(1 - b)_i$  parameters moving towards higher values for higher redshift.

The CCCP and WtG analysis provide results regarding a mass dependence for the mass bias, while not discussing a possible redshift dependence. Both WtG and CCCP agree on finding a modest evidence for the mass dependence, having  $M_{\text{Planck}} \propto M_{\text{WtG}}^{0.76+0.39}_{-0.20}$  and  $M_{\text{Planck}} \propto M_{\text{CCCP}}^{0.64+0.017}$ .

In the collection of CoMaLit papers ([Sereno & Ettori 2015b](#); [Sereno et al. 2015](#); [Sereno 2015](#); [Sereno & Ettori 2015a, 2017](#)) the authors provide an extensive discussion on measurements and calibrations for the scaling relations, analyzing different wavelengths results. In particular, in [Sereno & Ettori \(2017\)](#), the authors focus on the analysis of a possible mass and redshift dependence for the mass bias, comparing WL and tSZ estimated masses for a subsample of the Planck cosmological catalogue of 135 galaxy clusters. Their analysis provides a bias that is nearly mass independent but decreases with redshift, implying the cluster masses to be strongly underestimated at higher redshift. We find consistent results when considering the PSZ2 C sample, cutting at  $z_{\text{min}} = 0.2$ .

In [Smith et al. \(2016\)](#), the authors evaluate masses for a subsample of 44 Planck clusters in the redshift range  $z = [0.15, 0.3]$ , finding the value  $(1 - b) = 0.95 \pm 0.04$ . When comparing this value with WtG and CCCP analyses, they find that the different results are due not only to different methods of mass calculation, but also to the different redshift ranges. Indeed, when splitting WtG and CCCP redshift ranges in two bins ( $z < 0.3$  and  $z > 0.3$ ) and re-evaluating clusters masses, they find a general agreement on the mass bias for the lower redshift bin, highlighting a decreasing trend with respect to redshift. We find, again, the same trend when considering the PSZ2 C sample, with  $z_{\text{min}} = 0.2$ .

Hence, we stress again the difficulty in comparing our results and the different analysis, since we have shown how the mass and redshift dependence may depend on the sample definition, providing a hint of different behaviour for low redshift ( $z < 0.2$ ) and high redshift ( $z > 0.2$ ) clusters. Therefore, in order to improve these results and provide a more realistic description of the mass-redshift

evolution of the mass bias, it is necessary to have access to WL calibrations based on wider subsamples, more representative of the cluster population that we are considering for the cosmological analysis.

We now focus on the evaluation of the mass bias from CMB and tSZ data combination. We have already discussed how the latest results on the optical depth from the Planck collaboration have significantly reduced the discrepancy on the  $\sigma_8$  parameter between tSZ and CMB data, up to  $1.5\sigma$  and, as a consequence, the one on the mass bias. Nevertheless, CMB primary anisotropies prefer values of the mass bias,  $(1-b) \simeq 0.6$ , that are still lower than WL calibrations.

We also compare the CMB+tSZ results on the mass bias with alternative estimates. We consider the analysis presented in Eckert et al. (2018), which provide constraints on the mass bias through the evaluation of non-thermal pressure contributions. The authors analyse how physical quantities that describe the intracluster medium deviate from the pure gravitational collapse model and therefore from the condition of hydrostatic equilibrium. In particular, they focus on the evaluation of the gas fraction for 12 local massive clusters in the Planck cosmological catalogue, from which they obtain the mass bias constraints  $(1-b) = 0.85 \pm 0.05$ . Furthermore, they stress how constant values of mass bias  $(1-b) \sim 0.6$  result in a too low value for the universal gas fraction, being rejected at almost  $4\sigma$ .

Therefore, in previous sections we have analysed if the mass-redshift parametrisation proposed in Eq 1 can help in shifting the mass bias constraints towards higher values, for the CMB+tSZ dataset combination. Nevertheless, when we apply the " $(1-b) + \alpha_b + \beta_b$ " parametrisation, we find results that are consistent with the standard scenario, having  $(1-b)_{\text{var}} \simeq 0.6$ . Furthermore, as shown in Fig. 5, the variation of  $(1-b)_{\text{var}}$  for tSZ data allows only for partial consistency between the two datasets combinations.

We conclude therefore that a possible mass-redshift parametrisation of the mass bias does not help in completely reconciling results from CMB and tSZ data, still providing constraints not in agreement with other astrophysical evaluations.

## 6. Conclusions

We analyse a possible dependence for the mass bias with respect to mass and redshift, considering galaxy clusters observed through the tSZ effect by the Planck satellite and combining galaxy clusters number counts with estimation of tSZ power spectrum. We compare and combine tSZ data with the latest CMB results from the Planck satellite.

We consider an empirical mass-redshift parametrisation and perform several tests in order to check the consistency of our results. When considering tSZ data, we find a hint for redshift dependence, leading the  $(1-b)_{\text{var}}$  quantity to increase with redshift. We test that these results do not depend on the choice of the WL calibrations, by comparing the effect of the CCCP and WtG calibrations. As a further test, we divide the redshift range for the PSZ2 cosmo sample in 3 bins and analyse the change in the  $(1-b)_i$  parameters. We find the same hint for redshift dependence, having the  $(1-b)_i$  parameters increasing towards higher redshift.

We stress however that these results depend on the selected cluster sample. Indeed we compare results from

samples obtained considering different signal-to-noise ratio thresholds and redshift range. In general, we find the constraints on  $\alpha_b$  and  $\beta_b$  (and therefore the mass and redshift dependence) to change for the different samples. It is therefore difficult to fully compare these results with other analyses available in literature.

We analyse results for the complete CMB+tSZ data combination. We find statistically consistent results on the  $(1-b)_{\text{var}}$  quantity. Nevertheless, we stress that CMB data still pushes towards low values of the mass bias, providing results not in agreement with numerical simulations and WL estimations.

We conclude therefore that a possible mass-redshift variation, at the current level of precision and accuracy of observations, does not solve the discrepancy on the mass bias calibration between CMB and large scale structure evaluations.

*Acknowledgements.* LS acknowledges support from the post-doctoral grant from Centre National d'Études Spatiales (CNES). AB acknowledges support from NSERC'S Discovery Grant program. Based on observations obtained with Planck (<http://www.esa.int/Planck>), an ESA science mission with instruments and contributions directly funded by ESA Member States, NASA, and Canada. This project made use of the SZ-Cluster Database ([http://szcluster-db.ias.u-psud.fr/sitools/client-user/SZCLUSTER\\_DATABASE/project-index.html](http://szcluster-db.ias.u-psud.fr/sitools/client-user/SZCLUSTER_DATABASE/project-index.html)) operated by the Integrated Data and Operation Centre (IDOC) at the Institut d'Astrophysique Spatiale (IAS) under contract with CNES and CNRS. This project has received funding from the European Research Council (ERC) under the European Union's Horizon 2020 research and innovation programme grant agreement ERC-2015-AdG 695561.

## References

- Anderson, L. et al. 2014, *Mon. Not. Roy. Astron. Soc.*, 441, 24  
 Biffi, V., Borgani, S., Murante, G., et al. 2016, *Astrophys. J.*, 827, 112  
 Bocquet, S. et al. 2018 [[arXiv:1812.01679](https://arxiv.org/abs/1812.01679)]  
 Böhringer, H., Chon, G., Retzlaff, J., et al. 2017, *Astron. J.*, 153, 220  
 de Haan, T. et al. 2016, *Astrophys. J.*, 832, 95  
 Eckert, D. et al. 2018 [[arXiv:1805.00034](https://arxiv.org/abs/1805.00034)]  
 George, E. M. et al. 2015, *Astrophys. J.*, 799, 177  
 Hoekstra, H., Herbonnet, R., Muzzin, A., et al. 2015, *Mon. Not. Roy. Astron. Soc.*, 449, 685  
 Hoekstra, H., Mahdavi, A., Babul, A., & Bildfell, C. 2012, *Mon. Not. Roy. Astron. Soc.*, 427, 1298  
 Lewis, A. & Bridle, S. 2002, *Phys. Rev.*, D66, 103511  
 Mahdavi, A., Hoekstra, H., Babul, A., et al. 2013, *Astrophys. J.*, 767, 116  
 Mahdavi, A., Hoekstra, H., Babul, A., & Henry, J. P. 2008, *Mon. Not. Roy. Astron. Soc.*, 384, 1567  
 McCarthy, I. G., Babul, A., Holder, G. P., & Balogh, M. L. 2003a, *Astrophys. J.*, 591, 515  
 McCarthy, I. G., Holder, G. P., Babul, A., & Balogh, M. L. 2003b, *Astrophys. J.*, 591, 526  
 Okabe, N. & Smith, G. P. 2016, *Mon. Not. Roy. Astron. Soc.*, 461, 3794  
 Pacaud, F. et al. 2018, *Astron. Astrophys.* [[arXiv:1810.01624](https://arxiv.org/abs/1810.01624)]  
 Penna-Lima, M., Bartlett, J. G., Rozo, E., et al. 2017, *Astron. Astrophys.*, 604, A89  
 Planck Collaboration. 2014, *A&A*, 571, A20  
 Planck Collaboration. 2016a, *A&A*, 594, A22  
 Planck Collaboration. 2016b, *A&A*, 594, A24  
 Planck Collaboration. 2016c, *A&A*, 594, A26  
 Planck Collaboration. 2016d, *A&A*, 596, A107  
 Planck Collaboration. 2018a [[arXiv:1807.06205](https://arxiv.org/abs/1807.06205)]  
 Planck Collaboration. 2018b [[arXiv:1807.06209](https://arxiv.org/abs/1807.06209)]  
 Poole, G. B., Babul, A., McCarthy, I. G., et al. 2007, *Mon. Not. Roy. Astron. Soc.*, 380, 437  
 Ruan, J. J., Quinn, T. R., & Babul, A. 2013, *Mon. Not. Roy. Astron. Soc.*, 432, 3508  
 Rykoff, E. S. et al. 2016, *Astrophys. J. Suppl.*, 224, 1

- Salvati, L., Douspis, M., & Aghanim, N. 2018, *Astron. Astrophys.*, 614, A13
- Sereno, M. 2015, *Mon. Not. Roy. Astron. Soc.*, 450, 3665
- Sereno, M., Covone, G., Izzo, L., et al. 2017, *Mon. Not. Roy. Astron. Soc.*, 472, 1946
- Sereno, M. & Ettori, S. 2015a, *Mon. Not. Roy. Astron. Soc.*, 450, 3675
- Sereno, M. & Ettori, S. 2015b, *Mon. Not. Roy. Astron. Soc.*, 450, 3633
- Sereno, M. & Ettori, S. 2017, *Mon. Not. Roy. Astron. Soc.*, 468, 3322
- Sereno, M., Ettori, S., & Moscardini, L. 2015, *Mon. Not. Roy. Astron. Soc.*, 450, 3649
- Smith, G. P. et al. 2016, *Mon. Not. Roy. Astron. Soc.*, 456, L74
- Sunyaev, R. A. & Zeldovich, Ya. B. 1970, *Astrophys. Space Sci.*, 7, 20
- Tinker, J., Kravtsov, A. V., Klypin, A., et al. 2008, *ApJ*, 688, 709
- von der Linden, A. et al. 2014, *Mon. Not. Roy. Astron. Soc.*, 443, 1973
- Zhang, Y.-Y. et al. 2010, *Astrophys. J.*, 711, 1033